Supplementary Information

Accelerated Design for Perovskite-Oxide-Based Photocatalysts Using Machine Learning Techniques

Xiuyun Zhai [1,*] and Mingtong Chen [2,*]

[1] College of Intelligent Manufacturing, Hunan University of Science and Engineering, Yongzhou 425199, China
[2] Public Experimental Teaching Center, Panzhihua University, Panzhihua 617000, China
* Correspondence: cqfbb2008@shu.edu.cn (X.Z.); cmt2711@126.com (M.C.)

Table S1 Overview of ML applications in ABO_3-type perovskites

No.	Target properties	Algorithms	Ref
1	Thermodynamic phase stability	ET and KRR	[1]
2	Stable and metastable	GBDT	[2]
3	Formability and cubic structure stability	RF and Gradient boosting tree	[3]
4	Formation energy and bandgap	GBR	[4]
5	Curie temperature	SVR	[5]
6	Curie temperature	RR, SVM and ERT	[6]
7	Néel temperature	SVM	[7]
8	Maximum magnetic entropy change	GPR	[8]
9	Ionic conductivity	SVM	[9]
10	Specific surface area	SVM	[10]
11	The nature of band gap	RF	[11]
12	Thermodynamic stable	PSO-SVR and SVR	[12]
13	Crystal structure	Boosting algorithms, KNN and XGBoost	[13]
14	Perovskite structures	Quantum Machine Learning	[14]
15	Formability of perovskite structures	GBDT	[15]
16	Formation energy	DTR, GBRT, RFR and ETR	[16]
17	Defect formation energy	RFR	[17]
18	Thermal expansion coefficient	SVM	[18]
19	Oxygen ionic conductivities	GPR	[19]
20	Formability and stability	RF	[20]
21	Experimental design	ANN, Gaussian process and SVR	[21]
22	Stability	PCA and LFA	[22]
23	Band gaps and Band-edge positions	GBDT, LRR and KRR	[23]
24	Hydrogen production rate	GBR, BPANN and SVR	[24]

Table S2 The dataset including 102 ABO_3-type perovskite samples

No.	Molecular formulas	***SSA*** (m^2g^{-1})	***CT*** (℃)	***AH*** (h)	*DT* (℃)	PM	Ref.
1	$ZnTiO_3$	1.05	900	2	120	1	[25]
2	$LaFeO_3$	1.08	900	4	150	3	[26]
3	$LaCo_{0.94}Mg_{0.06}O_3$	19	750	4	110	3	[27]
4	$LaCo_{0.90}Mg_{0.10}O_3$	21	750	4	110	3	[27]
5	$LaCo_{0.80}Mg_{0.20}O_3$	22	750	4	110	3	[27]
6	$La_{0.5}Bi_{0.2}Ba_{0.2}Mn_{0.1}FeO_3$	20.63	600	4	120	3	[28]
7	$La_{0.5}Bi_{0.2}Ba_{0.2}Mn_{0.1}FeO_3$	12.46	700	4	120	3	[28]
8	$La_{0.5}Bi_{0.2}Ba_{0.2}Mn_{0.1}FeO_3$	5.91	800	4	120	3	[28]
9	$La_{0.5}Bi_{0.2}Ba_{0.2}Mn_{0.1}FeO_3$	4.19	900	4	120	3	[28]
10	$LaCrO_3$	3.95	600	5	100	3	[29]
11	$LaMg_{0.2}Cr_{0.8}O_3$	8.42	600	5	100	3	[29]
12	$LaMg_{0.4}Cr_{0.6}O_3$	29.71	600	5	100	3	[29]
13	$LaMg_{0.6}Cr_{0.4}O_3$	18.41	600	5	100	3	[29]
14	$LaMg_{0.8}Cr_{0.2}O_3$	14.46	600	5	100	3	[29]
15	$PrFeO_3$	10.88	700	5	90	3	[30]
16	$LaFe_{0.9}Co_{0.1}O_3$	51.2	750	10	110	3	[31]
17	$LaFe_{0.1}Co_{0.9}O_3$	42.8	750	10	110	3	[31]
18	$SrTiO_3$	16.4	650	10	110	3	[32]
19	$La_{0.002}Sr_{0.998}TiO_3$	19.7	650	10	110	3	[32]
20	$La_{0.01}Sr_{0.99}TiO_3$	24.1	650	10	110	3	[32]
21	$La_{0.02}Sr_{0.98}TiO_3$	23.2	650	10	110	3	[32]
22	$LaNiO_3$	14.1	600	2	130	2	[33]
23	$LaNiO_3$	12.7	700	2	130	2	[33]
24	$LaNiO_3$	11.8	800	2	130	2	[33]
25	$LaNiO_3$	6.5	900	2	130	2	[33]
26	$LaNiO_3$	12.2	600	6	130	2	[33]
27	$LaFeO_3$	21.9	500	4	120	3	[34]
28	$LaFeO_3$	15.37	600	4	120	3	[34]
29	$LaFeO_3$	10.07	700	4	120	3	[34]
30	$LaFeO_3$	5.24	800	4	120	3	[34]
31	$SrTiO_3$	12.24	700	4	80	1	[35]
32	$SrTiO_3$	10	700	4	80	1	[36]
33	$LaCuO_3$	5	800	15	100	3	[37]
34	$LaCu_{0.53}Ni_{0.47}O_3$	8.2	800	15	100	3	[37]
35	$La_{0.8}Sr_{0.2}Ni_{0.8}Cu_{0.2}O_3$	9	700	5	100	3	[38]
36	$La_{0.8}Sr_{0.2}Ni_{0.8}Fe_{0.2}O_3$	13.9	700	5	100	3	[38]
37	$La_{0.8}Sr_{0.2}Ni_{0.8}Bi_{0.2}O_3$	12.1	700	5	100	3	[38]
38	$LaNiO_3$	7.5	750	5	100	3	[39]
39	$LaNi_{0.8}Fe_{0.2}O_3$	7.9	750	5	100	3	[39]
40	$LaNi_{0.6}Fe_{0.4}O_3$	9.6	750	5	100	3	[39]
41	$LaNi_{0.3}Fe_{0.7}O_3$	6.8	750	5	100	3	[39]
42	$LaFeO_3$	15.1	750	5	100	3	[39]
43	$LaFeO_3$	25.8	500	2	130	2	[40]
44	$LaFeO_3$	22.55	600	2	130	2	[40]

No.	Molecular formulas	***SSA*** (m^2g^{-1})	***CT*** (℃)	***AH*** (h)	*DT* (℃)	PM	Ref.
45	$LaFeO_3$	20.04	700	2	130	2	[40]
46	$LaFeO_3$	8.5	800	2	130	2	[40]
47	$GaFeO_3$	56	600	8	300	1	[41]
48	$GaFeO_3$	38	700	8	300	1	[41]
49	$GaFeO_3$	10	900	8	300	1	[41]
50	$NaTaO_3$	2.25	900	12	120	3	[42]
51	$Na_{0.995}La_{0.005}TaO_3$	3.83	900	12	120	3	[42]
52	$Na_{0.985}La_{0.015}TaO_3$	4.55	900	12	120	3	[42]
53	$Na_{0.98}La_{0.02}TaO_3$	4.54	900	12	120	3	[42]
54	$Na_{0.95}La_{0.05}TaO_3$	4.36	900	12	120	3	[42]
55	$SrTiO_3$	16.2	900	4	80	3	[43]
56	$Ca_{0.98}Ag_{0.01}La_{0.01}TiO_3$	10.61	850	10	120	3	[44]
57	$Ca_{0.96}Ag_{0.02}La_{0.02}TiO_3$	11.39	850	10	120	3	[44]
58	$Ca_{0.94}Ag_{0.03}La_{0.03}TiO_3$	12.17	850	10	120	3	[44]
59	$Ca_{0.92}Ag_{0.04}La_{0.04}TiO_3$	11.44	850	10	120	3	[44]
60	$LaFeO_3$	9.5	700	4	90	3	[45]
61	$LaFeO_3$	11.39	600	5	150	3	[46]
62	$LaMg_{0.2}Fe_{0.8}O_3$	15.07	600	5	150	3	[46]
63	$LaMg_{0.4}Fe_{0.6}O_3$	17.63	600	5	150	3	[46]
64	$LaMg_{0.6}Fe_{0.4}O_3$	24.41	600	5	150	3	[46]
65	$LaMgO_3$	10.17	600	5	150	3	[46]
66	$PrCo_{0.7}Fe_{0.3}O_3$	7.9	700	2	90	3	[47]
67	$PrCo_{0.6}Fe_{0.4}O_3$	8.7	700	2	90	3	[47]
68	$PrCo_{0.5}Fe_{0.5}O_3$	7.5	700	2	90	3	[47]
69	$PrCo_{0.3}Fe_{0.7}O_3$	9.9	700	2	90	3	[47]
70	$PrCo_{0.1}Fe_{0.9}O_3$	9.7	400	2	90	3	[47]
71	$PrCo_{0.1}Fe_{0.9}O_3$	15.2	600	2	90	3	[47]
72	$PrCo_{0.1}Fe_{0.9}O_3$	15	700	2	90	3	[47]
73	$PrCo_{0.1}Fe_{0.9}O_3$	9.5	800	2	90	3	[47]
74	$LaMnO_3$	26	600	4	120	3	[48]
75	$LaFeO_3$	19	600	4	120	3	[48]
76	$LaCoO_3$	16	600	4	120	3	[48]
77	$LaCoO_3$	1.1	750	4	300	3	[49]
78	$LaCo_{0.8}Ru_{0.2}O_3$	2.9	750	4	300	3	[49]
79	$LaCo_{0.6}Ru_{0.4}O_3$	5	750	4	300	3	[49]
80	$LaAlO_3$	17.1	800	2	200	3	[50]
81	$LaAl_{0.9}Ni_{0.1}O_3$	6	800	2	200	3	[50]
82	$LaAl_{0.8}Ni_{0.2}O_3$	7	800	2	200	3	[50]
83	$LaAl_{0.7}Ni_{0.3}O_3$	6	800	2	200	3	[50]
84	$La_{0.9}Ca_{0.1}Al_{0.9}Ni_{0.1}O_3$	17	800	2	200	3	[50]
85	$La_{0.9}Ca_{0.1}Al_{0.8}Ni_{0.2}O_3$	15	800	2	200	3	[50]
86*	$LaCoO_3$	17	750	4	110	1	[27]
87*	$La_{0.5}Bi_{0.2}Ba_{0.2}Mn_{0.1}FeO_3$	27.75	500	4	120	1	[28]
88*	$LaFeO_3$	8.5	700	3	110	3	[51]
89*	$La_{0.005}Sr_{0.995}TiO_3$	22.3	650	10	110	3	[32]
90*	$LaNiO_3$	15.1	600	4	130	2	[33]

No.	Molecular formulas	***SSA*** (m^2g^{-1})	***CT*** (℃)	***AH*** (h)	***DT*** (℃)	PM	Ref.
91*	$LaFeO_3$	1.09	1000	4	120	1	[34]
92*	$La_{0.8}Sr_{0.2}Ni_{0.8}Co_{0.2}O_3$	10.3	700	5	100	3	[38]
93*	$LaFeO_3$	5.8	900	2	130	2	[40]
94*	$Na_{0.92}La_{0.08}TaO_3$	4.21	900	12	120	1	[42]
95*	$CaTiO_3$	9.64	850	10	120	1	[44]
96*	$LaMg_{0.8}Fe_{0.2}O_3$	13.32	600	5	150	3	[46]
97*	$PrCo_{0.9}Fe_{0.1}O_3$	7.2	700	2	90	3	[47]
98*	$PrCo_{0.1}Fe_{0.9}O_3$	19.3	500	2	90	1	[47]
99*	$La_{0.9}Ca_{0.1}Al_{0.7}Ni_{0.3}O_3$	12	800	2	200	3	[50]
100#	$LaFeO_3$	7	850	4	110	3	[52]
101#	$GdCoO_3$	8.69	750	4	110	3	[53]
102#	$LaMnO_3$	25	700	3	110	3	[54]

Table S3 The meanings of the twenty-five candidate features

No.	Meanings	Features	No.	Meanings	Features
1	Calcination Temperature (℃)	CT	14	Unit Cell Lattice Edge	α
2	Calcination Time (h)	AH	15	Enthalpy of fusion at the melting point of A-site (kJ/mol)	Δfus_A
3	Drying Temperature (℃)	DT	16	Enthalpy of fusion at the melting point of B-site (kJ/mol)	Δfus_B
4	Synthetic Mode	PM	17	Melting Point of A-site (℃)	T_{mA}
5	Ionic Radius of A-site (pm)	R_A	18	Melting Point of B-site (℃)	T_{mB}
6	Ionic Radius of B-site (pm)	R_B	19	Boiling Point of A-site (℃)	T_{bA}
7	Ratio of Ionic Radius	R_A/R_B	20	Boiling Point of B-site (℃)	T_{bB}
8	Tolerance Factor	T_f	21	Density of A-site (g/cm^3)	ρ_A
9	Molecular Mass (g/mol)	M	22	Density of B-site (g/cm^3)	ρ_B
10	Pauling Electronegativity of A-site	χ_{pA}	23	Electron Affinity of A-site (kJ/mol)	EA_a
11	Pauling Electronegativity of B-site	χ_{pB}	24	Electron Affinity of B-site (kJ/mol)	EA_b
12	Ionization Energy of A-site (eV)	Z_{IA}	25	Critical Radius	r_c
13	Ionization Energy of B-site (eV)	Z_{IB}			

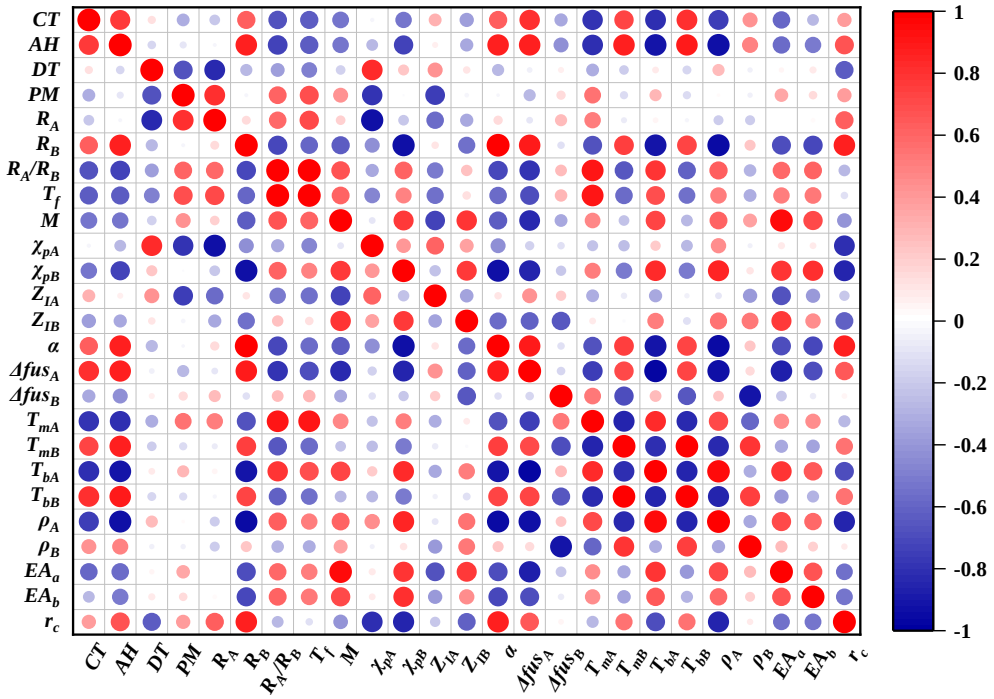

Figure S1 Pearson correlation matrix diagram of the twenty-five features

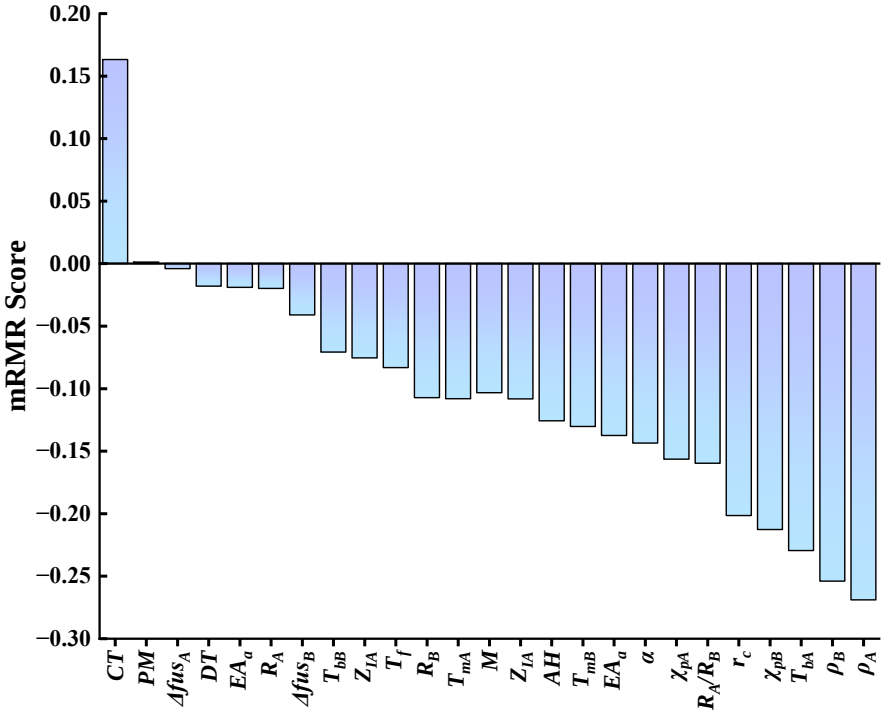

Figure S2 The mRMR scores of the twenty-five features

$$P_{CA1} = -0.259Z_{IA}+0.012EA_a+0.00365EA_b+0.00134T_{mA}-0.000692T_{mB}+0.000495T_{bA}-0.0105\Delta fus_A+0.2355\rho_A-0.00216CT-0.0934AH+5.448E-05DT+0.1657PM+0.3918 \quad (S1)$$

$$P_{CA2} = 1.252Z_{IA}-0.0176EA_a-0.00437EA_b+0.000174T_{mA}-0.000698T_{mB}-3.958E-05T_{bA}+0.00197\Delta fus_A+0.1162\rho_A-0.0004163CT-0.0859AH+0.003415DT-0.782PM-3.542 \quad (S2)$$

$$P_{CA3} = -0.1473Z_{IA}+0.01277EA_a+0.00852EA_b-0.001796T_{mA}+0.000290T_{mB}+3.97E-05T_{bA}-0.005132\Delta fus_A+0.07203\rho_A+0.00192\,CT+0.00353\,AH+0.01098DT-0.6485PM-0.1763 \quad (S3)$$

$$P_{CA4} = 0.3796Z_{IA}-0.006746EA_a+0.01845EA_b+0.001076T_{mA}-0.000336T_{mB}+6.914E-05T_{bA}+0.00348\Delta fus_A+0.003075\rho_A+0.00531\,CT+0.01077AH-0.001409DT+0.3009PM-7.915 \quad (S4)$$

$$P_{CA5} = 0.1268Z_{IA}-0.00104EA_a+0.0104EA_b-0.000318T_{mA}+0.0008359T_{mB}-7.796E-05T_{bA}-0.005807\Delta fus_A+0.01999\rho_A-0.001758CT-0.03819\,AH-0.01129DT-0.819PM+3.624 \quad (S5)$$

$$P_{CA6} = 0.591Z_{IA}+0.01055EA_a-0.01066EA_b-0.0006895T_{mA}+0.000652T_{mB}+1.383E-05T_{bA}-0.002944\Delta fus_A+0.1368\rho_A+0.004784CT-0.1168AH-0.00406DT+0.379PM-7.712 \quad (S6)$$

References

[1] Li, W.; Jacobs R.; Morgan D. Predicting the thermodynamic stability of perovskite oxides using machine learning models. *Computational Materials Science* **2018**, 150, 454-463.

[2] Liu, H.Y.; Cheng J.C.; Dong H.Z.; Feng J.G.; Pang B.L.; Tian Z.Y.; Ma S.; Xia F.J.; Zhang C.K.; Dong L.F. Screening stable and metastable ABO_3 perovskites using machine learning and the materials project. *Computational Materials Science* **2020**, 177, 109614.

[3] Balachandran, P.V.; Emery A.A.; Gubernatis J.E.; Lookman T.; Wolverton C.; Zunger A. Predictions of new ABO_3 perovskite compounds by combining machine learning and density functional theory. *Physical Review Materials* **2018**, 2, 043802.

[4] Li, C.J.; Hao H.; Xu B.; Zhao G.H.; Chen L.H.; Zhang S.J.; Liu H.X. A progressive learning method for predicting the band gap of ABO_3 perovskites using an instrumental variable.

Journal of Materials Chemistry C **2020**, 8, 3127-3136.

[5] Zhai, X.Y.; Chen M.T.; Lu W.C. Accelerated search for perovskite materials with higher Curie temperature based on the machine learning methods. *Computational Materials Science* **2018**, 151, 41-48.

[6] Yang, Z.X.; Gao Z.R.; Sun X.F.; Cai H.L.; Zhang F.M.; Wu X.S. High critical transition temperature of lead-based perovskite ferroelectric crystals: A machine learning study. *Acta Physica Sinica* **2019**, 68, 210502.

[7] Xiao L.H., Z.Q., Xu X., Ji X.B. and Lu W.C. Support vector regression assisted predictions the néel temperature of perovskites manganites. *Computers and Applied Chemistry* **2018**, 35, 349-357.

[8] Zhang, Y.; Xu X.J. Machine learning the magnetocaloric effect in manganites from lattice parameters. *Applied Physics A-materials Science & Processing* **2020**, 126, 341.

[9] Xu, L.; Wencong L.; Chunrong P.; Qiang S.; Jin G. Two semi-empirical approaches for the prediction of oxide ionic conductivities in ABO_3 perovskites. *Computational Materials Science* **2009**, 46, 860-868.

[10] Shi, L.; Chang D.P.; Ji X.B.; Lu W.C. Using Data Mining To Search for Perovskite Materials with Higher Specific Surface Area. *Journal of Chemical Information and Modeling* **2018**, 58, 2420-2427.

[11] Priyanga, G.S.; Mattur M.N.; Nagappan N.; Rath S.; Thomas T. Prediction of nature of band gap of perovskite oxides (ABO_3) using a machine learning approach. *Journal of Materiomics* **2022**, 8, 937-948.

[12] Chen, L.P.; Wang X.C.; Xia W.J.; Liu C.H. PSO-SVR predicting for the Ehull of ABO_3-type compounds to screen the thermodynamic stable perovskite candidates based on multi-scale descriptors. *Computational Materials Science* **2022**, 211, 111435.

[13] Priyadarshini, R.; Joardar H.; Bisoy S.K.; Badapanda T. Crystal structural prediction of perovskite materials using machine learning: A comparative study. *Solid State Communications* **2023**, 361, 115062.

[14] Naseri, M.; Gusarov S.; Salahub D.R. Quantum Machine Learning in Materials Prediction: A Case Study on ABO_3 Perovskite Structures. *Journal of Physical Chemistry Letters* **2023**, 14, 6940-6947.

[15] Chen, L.P.; Xia W.J.; Yao T.Z. Identifying descriptors for perovskite structure of composite oxides and inferring formability via low-dimensional described features. *Computational Materials Science* **2023**, 226, 112216.

[16] Fan, X.Y. Prediction Of Formation Energy Using Two-Stage Machine Learning Based On Clustering. *Materiali In Tehnologije* **2021**, 55, 263-268.

[17] Sharma, V.; Kumar P.; Dev P.; Pilania G. Machine learning substitutional defect formation energies in ABO_3 perovskites. *Journal Of Applied Physics* **2020**, 128.

[18] McGuinness, K.P.; Oliynyk A.O.; Lee S.; Molero-Sanchez B.; Addo P.K. Machine-learning prediction of thermal expansion coefficient for perovskite oxides with experimental validation. *Physical Chemistry Chemical Physics* **2023**, 25, 32123-32131.

[19] Zhang, Y.; Xu X.J. Modeling oxygen ionic conductivities of ABO_3 Perovskites through machine learning. *Chemical Physics* **2022**, 558, 111511.

[20] Zhao, J.; Wang X.Y. Screening Perovskites from ABO_3 Combinations Generated by Constraint Satisfaction Techniques Using Machine Learning. *ACS Omega* **2022**, 7, 10483-

10491.

[21] Lourenço, M.P.; Tchagang A.; Shankar K.; Thangadurai V.; Salahub D.R. Active learning for optimum experimental design--insight into perovskite oxides. *Canadian Journal Of Chemistry* **2023**, 101, 734-744.

[22] Bhattacharya, S.; Roy A. Linking stability with molecular geometries of perovskites and lanthanide richness using machine learning methods. *Computational Materials Science* **2024**, 231, 112581.

[23] Li, W.; Wang Z.G.; Xiao X.; Zhang Z.Q.; Janotti A.; Rajasekaran S.; Medasani B. Predicting band gaps and band-edge positions of oxide perovskites using density functional theory and machine learning. *Physical Review B* **2022**, 106, 155156.

[24] Tao, Q.L.; Chang D.P.; Lu T.; Li L.; Chen H.M.; Yang X.; Liu X.J.; Li M.J.; Lu W.C. Multiobjective Stepwise Design Strategy-Assisted Design of High-Performance Perovskite Oxide Photocatalysts. *Journal of Physical Chemistry C* **2021**, 125, 21141-21150.

[25] Perween, S.; Ranjan A. Improved visible-light photocatalytic activity in $ZnTiO_3$ nanopowder prepared by sol-electrospinning. *Solar Energy Materials and Solar Cells* **2017**, 163, 148-156.

[26] Orak, C.; Atalay S.; Ersöz G. Photocatalytic and photo-Fenton-like degradation of methylparaben on monolith-supported perovskite-type catalysts. *Separation Science and Technology* **2017**, 52, 1310-1320.

[27] Sun, H.; Yang H.; Cui S.; Nie K.; Wu J. Simultaneous Mg-Modification Inside and Outside of $LaCoO_3$ Lattice and Their Photocatalytic Properties. *Chinese Journal of Inorganic Chemistry* **2016**, 32, 1704-1712.

[28] Abdulkadir, I.; Jonnalagadda S.B.; Martincigh B.S. Synthesis and effect of annealing temperature on the structural, magnetic and photocatalytic properties of $(La_{0.5}Bi_{0.2}Ba_{0.2}Mn_{0.1})FeO_{(3-\delta)}$. *Materials Chemistry and Physics* **2016**, 178, 196-203.

[29] Josephine, B.A.; Manikandan A.; Teresita V.M.; Antony S.A. Fundamental study of $LaMg_xCr_{1-x}\ O_{3-\delta}$ perovskites nano-photocatalysts: sol-gel synthesis, characterization and humidity sensing. *Korean Journal of Chemical Engineering* **2016**, 33, 1590-1598.

[30] Tijare, S.N.; Bakardjieva S.; Subrt J.; Joshi M.V.; Rayalu S.S.; Hishita S.; Labhsetwar N. Synthesis and visible light photocatalytic activity of nanocrystalline $PrFeO_3$ perovskite for hydrogen generation in ethanol-water system. *Journal of Chemical Sciences* **2014**, 126, 517-525.

[31] Tavakkoli, H.; Yazdanbakhsh M. Fabrication of two perovskite-type oxide nanoparticles as the new adsorbents in efficient removal of a pesticide from aqueous solutions: Kinetic, thermodynamic, and adsorption studies. *Microporous and Mesoporous Materials* **2013**, 176, 86-94.

[32] Li, H.; Cui Y.; Wu X.; Hong W.; Hua L. Effect of La contents on the structure and photocatalytic activity of La-$SrTiO_3$ catalysts. *Chinese Journal of Inorganic Chemistry*, 28, 2597-2604.

[33] Li, Y.; Yao S.; Wen W.; Xue L.; Yan Y. Sol–gel combustion synthesis and visible-light-driven photocatalytic property of perovskite $LaNiO_3$. *Journal of Alloys and Compounds* **2010**, 491, 560-564.

[34] Li, S.; Jing L.; Fu W.; Yang L.; Xin B.; Fu H. Photoinduced charge property of nanosized perovskite-type $LaFeO_3$ and its relationships with photocatalytic activity under visible

irradiation. *Materials Research Bulletin* **2007**, 42, 203-212.

[35] Puangpetch, T.; Sreethawong T.; Chavadej S. Hydrogen production over metal-loaded mesoporous-assembled $SrTiO_3$ nanocrystal photocatalysts: Effects of metal type and loading. *International Journal of Hydrogen Energy* **2010**, 35, 6531-6540.

[36] Puangpetch, T.; Sreethawong T.; Yoshikawa S.; Chavadej S. Hydrogen production from photocatalytic water splitting over mesoporous-assembled $SrTiO_3$ nanocrystal-based photocatalysts. *Journal of Molecular Catalysis A: Chemical* **2009**, 312, 97-106.

[37] Touahra, F.; Rabahi A.; Chebout R.; Boudjemaa A.; Lerari D.; Sehailia M.; Halliche D.; Bachari K. Enhanced catalytic behaviour of surface dispersed nickel on $LaCuO_3$ perovskite in the production of syngas: an expedient approach to carbon resistance during CO_2 reforming of methane. *International Journal of Hydrogen Energy* **2016**, 41, 2477-2486.

[38] Sutthiumporn, K.; Maneerung T.; Kathiraser Y.; Kawi S. CO_2 dry-reforming of methane over $La_{0.8}Sr_{0.2}Ni_{0.8}M_{0.2}O_3$ perovskite (M = Bi, Co, Cr, Cu, Fe): Roles of lattice oxygen on C–H activation and carbon suppression. *International Journal of Hydrogen Energy* **2012**, 37, 11195-11207.

[39] Luo, Y.; Wang X.; Qian Q.; Chen Q. Studies on B sites in Fe-doped $LaNiO_3$ perovskite for SCR of NO_x with H_2. *International Journal of Hydrogen Energy* **2014**, 39, 15836-15843.

[40] Parida, K.M.; Reddy K.H.; Martha S.; Das D.P.; Biswal N. Fabrication of nanocrystalline $LaFeO_3$: An efficient sol–gel auto-combustion assisted visible light responsive photocatalyst for water decomposition. *International Journal of Hydrogen Energy* **2010**, 35, 12161-12168.

[41] Dhanasekaran, P.; Gupta N.M. Factors affecting the production of H_2 by water splitting over a novel visible-light-driven photocatalyst $GaFeO_3$. *International Journal of Hydrogen Energy* **2012**, 37, 4897-4907.

[42] Husin, H.; Chen H.-M.; Su W.-N.; Pan C.-J.; Chuang W.-T.; Sheu H.-S.; Hwang B.-J. Green fabrication of La-doped $NaTaO_3$ via H_2O_2 assisted sol–gel route for photocatalytic hydrogen production. *Applied Catalysis B: Environmental* **2011**, 102, 343-351.

[43] Bui, D.-N.; Mu J.; Wang L.; Kang S.-Z.; Li X. Preparation of Cu-loaded $SrTiO_3$ nanoparticles and their photocatalytic activity for hydrogen evolution from methanol aqueous solution. *Applied Surface Science* **2013**, 274, 328-333.

[44] Zhang, H.; Chen G.; He X.; Xu J. Electronic structure and photocatalytic properties of Ag–La codoped $CaTiO_3$. *Journal of Alloys and Compounds* **2012**, 516, 91-95.

[45] Tijare, S.N.; Joshi M.V.; Padole P.S.; Mangrulkar P.A.; Rayalu S.S.; Labhsetwar N.K. Photocatalytic hydrogen generation through water splitting on nano-crystalline $LaFeO_3$ perovskite. *International Journal of Hydrogen Energy* **2012**, 37, 10451-10456.

[46] Teresita, V.M.; Manikandan A.; Josephine B.A.; Sujatha S.; Antony S.A. Electromagnetic properties and humidity-sensing studies of magnetically recoverable $LaMg_xFe_{1-x}O_{3-\delta}$ perovskites nano-photocatalysts by Sol-Gel route. *Journal of Superconductivity and Novel Magnetism* **2016**, 29, 1691-1701.

[47] Sydorchuk, V.; Lutsyuk I.; Shved V.; Hreb V.; Kondyr A.; Zakutevskyy O.; Vasylechko L. $PrCo_{1-x}Fe_xO_3$ perovskite powders for possible photocatalytic applications. *Research on Chemical Intermediates* **2020**, 46, 1909-1930.

[48] Ibarra-Rodriguez, L.I.; Huerta-Flores A.M.; Mora-Hernandez J.M.; Torres-Martínez L.M. Photocatalytic evolution of H_2 over visible-light active $LaMO_3$(M: Co, Mn, Fe) perovskite

materials: Roles of oxygenated species in catalytic performance. *Journal of Physics and Chemistry of Solids* **2020**, 136, 109189.

[49] Mota, N.; Álvarez-Galván M.C.; Al-Zahrani S.M.; Navarro R.M.; Fierro J.L.G. Diesel fuel reforming over catalysts derived from $LaCo_{1-x}Ru_xO_3$ perovskites with high Ru loading. *International Journal of Hydrogen Energy* **2012**, 37, 7056-7066.

[50] Agüero, F.N.; Morales M.R.; Larrégola S.; Izurieta E.M.; Lopez E.; Cadús L.E. $La_{1-x}Ca_xAl_{1-y}NiyO_3$ perovskites used as precursors of nickel based catalysts for ethanol steam reforming. *International Journal of Hydrogen Energy* **2015**, 40, 15510-15520.

[51] Hu, R.; Li C.; Wang X.; Sun Y.; Jia H.; Su H.; Zhang Y. Photocatalytic activities of $LaFeO_3$ and La_2FeTiO_6 in p-chlorophenol degradation under visible light. *Catalysis Communications* **2012**, 29, 35-39.

[52] Boumaza, S.; Boudjellal L.; Brahimi R.; Belhadi A.; Trari M. Synthesis by citrates sol-gel method and characterization of the perovskite $LaFeO_3$: application to oxygen photo-production. *Journal of Sol-Gel Science and Technology* **2020**, 94, 486-492.

[53] Wang, J.; Li X.D.; Yu Z.Q.; Zhang S. Enhancing infrared emissivity of $GdCoO_3$ with Ca doping: Potential for advanced thermal control materials. *Ceramics International* **2024**, 50, 9630-9639.

[54] Guo, J.X.; Jing Y.; Shen T.; Luo H.D.; Liang J.; Yuan S.D. Effect of doped strontium on catalytic properties of $La_{1-x}Sr_xMnO_3$ for rhodamine B degradation. *Journal of Rare Earths* **2021**, 39, 1362-1369.